RSC Advances

ROYAL SOCIETY OF CHEMISTRY

PAPER

View Article Online
View Journal | View Issue

Check for updates

Cite this: *RSC Adv.*, 2026, **16**, 11655

Degradation of rhodamine B using a heterogeneous Fenton-like reaction driven by nano-zero-valent iron loaded on biochar prepared in the presence of ultrasonic irradiation

Xin-Yu Yang,[a] Hong-Xi Zhang,[a] Xun Dai,[a] Hao-Jie Zhang,[a] Ye Zhang,*[b] Dan Sun*[a] and Wei-Liang Tian*[a]

Received 9th December 2025
Accepted 15th February 2026

DOI: 10.1039/d5ra09509c

rsc.li/rsc-advances

The biochar-supported nanoscale zero-valent iron (nZVI@BC) was synthesized in the presence of ultrasonic irradiation and applied in the heterogeneous Fenton-like degradation of rhodamine B (RhB). The property changes in the nZVI@BC synthesized in the presence and absence of ultrasonic irradiation were characterized, which confirmed that the ultrasonically irradiated catalyst had a better dispersion and higher electron transfer rate, showing better catalytic performance for RhB degradation. The effects of the catalyst dosage, pH value and H_2O_2 concentration were investigated, and it was found that under the conditions of initial pH = 3, H_2O_2 concentration = 15 mmol L^{-1}, catalyst dosage = 1.5 g L^{-1} and 298 K, the RhB removal efficiency of nZVI@BC(ultrasonic irradiation) was 97.7%. Furthermore, the classical second-order kinetic model showed better fitting results, suggesting that the RhB degradation was primarily controlled by a chemical reaction, and the activation energy was calculated to be 77.8 kJ mol^{-1}. Based on quenching experiments and electron paramagnetic resonance spectra, free radicals $^{\bullet}OH$ and $^{\bullet}O_2^-$ were detected, and $^{\bullet}OH$ was found to be the main free radical in RhB degradation. After three cycles of catalyst reuse, its removal efficiency was still more than 70%. This work provides a new route for using ultrasonic irradiation to improve the catalyst performance in Fenton-like systems.

1. Introduction

Industrial dyes pose a significant threat to aquatic ecosystems due to their high stability, carcinogenicity and mutagenicity.[1,2] With the rapid growth of the dyeing and textile industries, large quantities of dye-containing wastewater are discharged into the environment. Rhodamine B (RhB) is used in textile dyeing and biological staining, and it is recalcitrant to the traditional biological treatment methods because of its complex aromatic structure and high chemical stability.[3,4] Consequently, the development of efficient technologies for RhB removal is of great significance.

Advanced oxidation processes (AOPs) have demonstrated significant potential in degrading recalcitrant organic compounds,[5] and the Fenton reaction has garnered extensive attention for its ability to generate highly reactive hydroxyl radicals ($^{\bullet}OH$) through the reaction of Fe^{2+} with hydrogen peroxide (H_2O_2).[6–8] However, the traditional homogeneous Fenton reaction suffers from several limitations, such as a narrow pH range (2–3), the generation of large amounts of iron sludge, and the difficulty in recycling the iron catalysts.[9] To overcome these limitations, heterogeneous Fenton-like systems have emerged as promising alternatives, which use iron-based solid catalysts instead of soluble iron salts, and these systems offer a broader applicable pH range and improved catalyst recyclability, thus significantly reducing the risk of secondary pollution.[10–12]

Studies have shown that nanoscale zero-valent iron (nZVI) has a high reduction potential and is easy to prepare, and it can react with H_2O_2 to form a heterogeneous Fenton-like system (nZVI/H_2O_2) for efficiently degrading pollutants.[13,14] However, the nZVI particles exhibit a tendency to aggregate into chain-like structures due to their small size and strong magnetic force, leading to a decrease in the reaction activity.[15–17] Additionally, nZVI particles are easily oxidized to form an oxide film, which can prevent direct contact between Fe^0 and pollutants.[18] Therefore, researchers have tried to use carriers, such as bentonite,[19] kaolinite,[20] activated carbon[21] and biochar(BC),[22] to stabilize nZVI and slow particle agglomeration. Among them, BC is a porous material with a stable structure and excellent adsorption capacity, and it has been widely used as a carrier material. A solid catalyst composed of nZVI loaded onto BC may

---

[a] *College of Chemistry and Chemical Engineering, Tarim University, Alar 843300, China. E-mail: sundan2991@163.com; twllong@126.com*

[b] *Xinjiang Key Laboratory of New Functional Materials, College of Chemical and Environmental Sciences, Kashi University, Kashi 844000, China. E-mail: zy992999214@163.com*

combine the advantages of both materials, and the RhB molecules may be adsorbed onto the BC surface and degraded at the solid–liquid interface *via* the Fenton-like oxidation system. Moreover, such a solid catalyst may be recycled with an external magnet.

Ultrasonic irradiation is a green and efficient method that can improve the degradation performance of a catalyst. Ultrasound has an acoustic cavitation effect,[23,24] which can promote the dispersion of nZVI. Meanwhile, the extremely intense shock waves can break the oxide film on the nZVI surface, exposing the inner Fe^0 core.[25] Thus, the biochar-supported nZVI catalyst (nZVI@BC) prepared in the presence of ultrasonic irradiation can enhance mass transfer, prevent the agglomeration of nZVI particles, and further improve the catalyst performance in the heterogeneous Fenton-like reaction.

In this study, the nZVI@BC catalyst was prepared under ultrasonic irradiation, and the influence of ultrasonic irradiation on the preparation of nZVI@BC was explored. The optimization of the process parameters was performed using batch experiments, and the potential of the nZVI@BC(ultrasonic irradiation)/H_2O_2 heterogeneous Fenton-like system for RhB removal was evaluated by kinetic analysis. Finally, based on catalyst characterization and active species identification, a removal mechanism for RhB was proposed. This research is expected to provide a new method and a theoretical basis for the efficient removal of RhB, offering valuable insights to guide the design of high-performance, sustainable Fenton-like catalysts.

2. Materials and methods

2.1 Materials and reagents

The samples of corncob were obtained from Xinjiang Alar, China. Chemicals, including iron chloride hexahydrate ($FeCl_3\cdot6H_2O$), sodium borohydride ($NaBH_4$), hydrogen peroxide (H_2O_2), and hydrochloric acid (HCl), were purchased from Sinopharm Group Chemical Reagent Co., Ltd, China. Sodium hydroxide (NaOH) and ethanol (C_2H_6O) were bought from Aladdin Reagent Co., Ltd, China. Rhodamine B ($C_{28}H_{31}ClN_2O_3$) and tertiary butanol ($C_4H_{10}O$) were purchased from Beijing Solepol Technology Co., Ltd, China.

2.2 Synthesis of the catalyst

The collected corncob was cleaned with deionized water and dried in an electric heating blower drying oven at 60 °C for 24 h. Then, the corncob was crushed *via* a crusher and passed through a 40-mesh sieve. The pre-treated corncob powder was placed in a muffle furnace for pyrolysis at 400 °C for 2 h under a nitrogen atmosphere to obtain biochar (BC), which was used for the subsequent material preparation. Under ultrasonic irradiation (KQ3200DB, 40 KHz, 150 W) and nitrogen protection, the nZVI@BC catalyst was prepared as follows: 0.5 g of BC and 2.5 g of $FeCl_3\cdot6H_2O$ were added into a 250-mL three-neck flask, and 100 mL of deionized water was poured to evenly mix the reactants, followed by ultrasonic stirring for 10 min. Freshly prepared $NaBH_4$ (0.58 g in 50 mL of deionized water) was progressively added to the mixture. Then, the stirring reaction was conducted in an ultrasonic bath at 30 °C for 40 min. The obtained black solid was washed three times with deionized water and ethanol with magnetic separation. Finally, the solid–liquid mixture was centrifuged at 8000 rpm for 5 min, the supernatant was carefully decanted, and the wet solid was dried in a vacuum drying box at 50 °C for 8 h to obtain the nZVI@BC catalyst.

2.3 Measurement and characterization techniques

The morphologies and surface elements of the prepared samples were observed *via* scanning electron microscopy (SEM, ZEISS Sigma 300, Germany), and the phase structures of the samples were identified by an X-ray diffractometer (XRD, UItima, Japan), with Cu K_α radiation ($\lambda = 0.15406$ nm) in the scanning range from 5° to 80°. The hysteresis loops of the nZVI@BC prepared in the presence and absence of ultrasonic irradiation were measured using a vibrating sample magnetometer (LakeShore7404). The specific surface area was measured using a surface area analyzer (Micromeritics ASAP2460, USA). The surface components of nZVI@BC were detected by X-ray photoelectron spectroscopy (XPS, Axis Supra, Britain). A micro-Raman spectroscopy system (inVia-Reflex, Britain) was used to record Raman spectra at an excitation wavelength of 514 nm. All electrochemical measurements were conducted on a CHI 760 E electrochemical workstation utilizing a three-electrode system, wherein the prepared sample was deposited on a glassy carbon working electrode, a Pt electrode served as the counter electrode, and an Ag/AgCl electrode was employed as the reference electrode. A 0.5 mol L^{-1} Na_2SO_4 solution was used as the electrolyte solution. The free radicals generated in the Fenton-like reaction were detected by an electron paramagnetic resonance (EPR) spectrometer (Bruker EMX-500 10/12, Germany).

2.4 Degradation experiments

The experiments were conducted in a 150-mL beaker containing 100 mL of an RhB solution (100 mg L^{-1}), and the initial pH was adjusted using 0.1 mol L^{-1} HCl and NaOH. Subsequently, predetermined amounts of the nZVI@BC catalyst and H_2O_2 were simultaneously introduced into the solution to initiate the degradation reaction. The beaker was placed in a shaker, the temperature was set at 25 °C, and the rotational speed was set at 150 r min^{-1}. Then, 1.0 mL of the reaction solution filtered through a 0.45-μm polytetrafluoroethylene syringe membrane was taken at a given time, and the residual radicals in the solution were immediately quenched with 20 μL of tert-butanol (TBA). The maximum absorbance of the filtrate was determined at 554 nm using a UV-vis spectrometer (UV-2501PC) and used to calculate the equilibrium concentration of RhB. The removal experiments were performed in triplicate.

2.5 Kinetics for RhB removal

The removal data were fitted by the classical first-order kinetic model (eqn (1)) and the second-order kinetic model (eqn (2)), which can be described as follows:[26,27]

$$\ln(C_t/C_0) = -k_1 t \tag{1}$$

$$1/C_t - 1/C_0 = k_2 t, \tag{2}$$

where C_0 and C_t (mg L^{-1}) are the initial RhB concentration and the RhB concentration at time t, respectively; and k_1 (min^{-1}) and k_2 (L mg^{-1} min^{-1}) are the kinetic rate constants of first and second order, respectively. In addition, based on previous studies, the activation energy (E_a, J mol^{-1}) of the RhB degradation reaction was calculated using the Arrhenius formula (eqn (3)),[28] where k is the rate constant and A_0 is the frequency coefficient, and the slope of the curve of $\ln k$ *versus* $1/T$ can be used to calculate E_a:

$$\ln k = -E_a/RT + \ln A_0 \tag{3}$$

3. Results and discussion

3.1 Characterization

As can be seen from Fig. 1a, BC had a large skeleton structure with a rough surface, and an obvious pore structure was also observed, which provided more space for loading nZVI particles. Fig. 1b shows that nZVI particles had a predominantly spherical structure with a uniform shape and size, but obvious agglomeration had occurred due to their high surface energy and mutual magnetic attraction; hence, the nZVI particles were tightly connected to each other in the form of chain clusters, which affected the removal performance of the material.[29] Fig. 1c and d show the SEM images of nZVI@BC prepared in the presence and absence of ultrasonic irradiation, respectively. Both the skeleton of BC and the distributed nZVI particles were observed in the two samples. According to the EDS results of the two samples, the main constituent elements were Fe, O and C, and the proportion of the Fe element was 31.3% and 32.85%, respectively. However, the nZVI in the ultrasonically irradiated nZVI@BC was uniformly distributed on BC, whereas the nZVI@BC prepared in the absence of ultrasonic irradiation showed that the loaded nZVI particles still had a lot of aggregates. Moreover, based on Scherrer's equation,[30] the nZVI@BC synthesized in the presence and absence of ultrasonic irradiation had average crystalline sizes of 6.4 nm and 9.7 nm, respectively, indicating that ultrasonic application augmented the dispersion of nZVI particles, and more active sites were exposed. Ultrasound produced strong shock waves as it propagated through the liquid, and the energy of the shock wave was

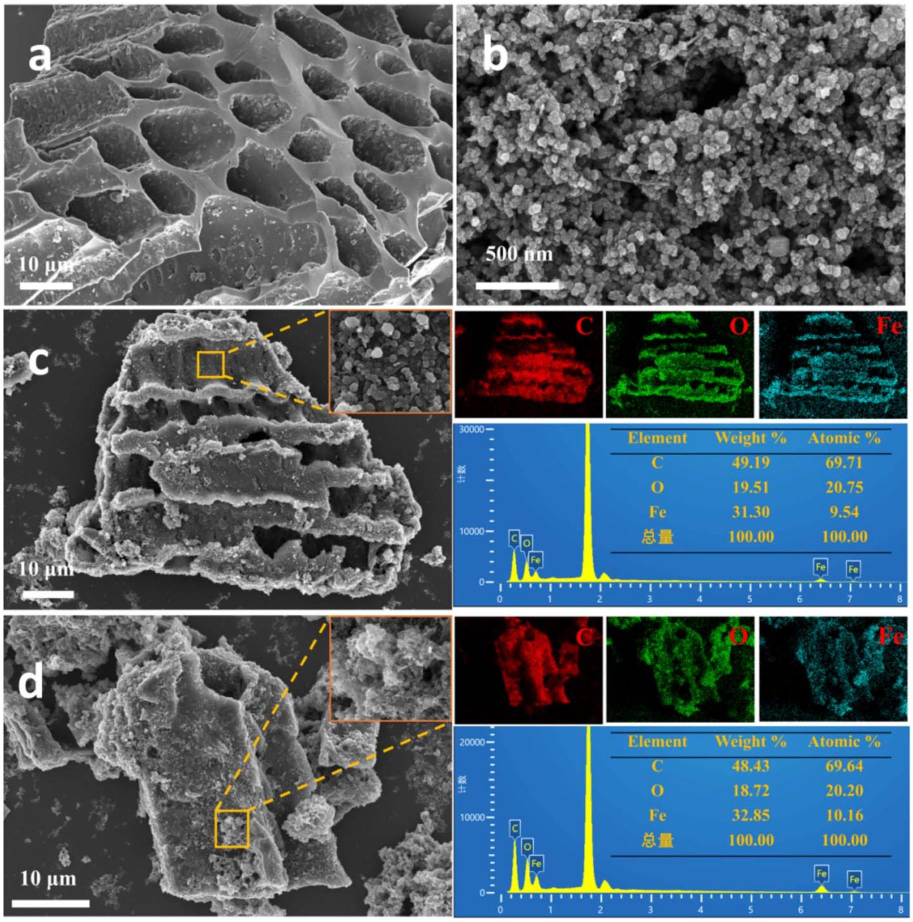

Element	Weight %	Atomic %
C	49.19	69.71
O	19.51	20.75
Fe	31.30	9.54
总量	100.00	100.00

Element	Weight %	Atomic %
C	48.43	69.64
O	18.72	20.20
Fe	32.85	10.16
总量	100.00	100.00

Fig. 1 SEM images of (a) BC, (b) nZVI, (c) nZVI@BC prepared in the presence of ultrasonic irradiation and EDS elemental mapping and (d) nZVI@BC prepared in the absence of ultrasonic irradiation and EDS elemental mapping.

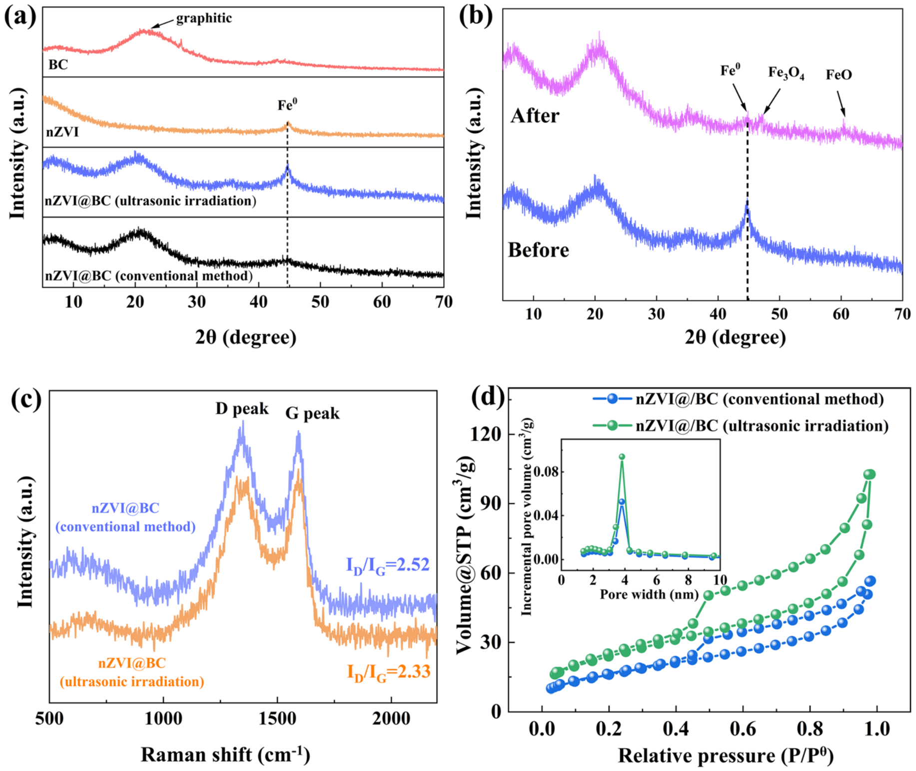

Fig. 2 (a) XRD patterns of the samples. (b) XRD patterns of the ultrasonically irradiated nZVI@BC before and after RhB degradation. (c) Raman spectra of the nZVI@BC prepared in the presence and absence of ultrasonic irradiation. (d) N_2 adsorption–desorption isotherms (inset: pore diameter distribution curves).

sufficient to destroy bonding forces, including van der Waals forces and magnetic attraction, which also pushed nZVI particles inside the voids of the BC and made the nZVI particles more uniformly distributed.[31] Therefore, the interaction between nZVI and the BC carrier was strengthened, and the effective active sites of nZVI were increased under ultrasonic irradiation.

The XRD patterns of the samples are shown in Fig. 2a. The BC showed a wide diffraction peak at 21.8°, attributed to the oxygen-containing functional groups of graphite, indicating that the prepared BC was graphitized.[32] nZVI showed an obvious characteristic peak at 44.9°, corresponding to the (110) crystal plane of Fe^0, and the Fe^0 characteristic peak was also found in the nZVI@BC prepared in the presence and absence of ultrasonic irradiation, showing that nZVI was successfully loaded onto the BC surface. In addition, compared with the ultrasonically irradiated nZVI@BC, the Fe^0 characteristic peak in the conventional-method-synthesized nZVI@BC was wider, and its peak intensity was also significantly reduced, suggesting that the crystallinity of Fe^0 was improved under ultrasonic irradiation, probably because the acoustic cavitation effect induced by ultrasound generated a localized environment with high temperatures and high pressures. This unique environment facilitated the uniform nucleation of Fe^0 to reduce initial defects and drove the oriented growth of nZVI grains. Furthermore, ultrasound inhibited the surface oxidation of nZVI and protected the integrity of its crystal lattice, which led to a significant improvement in the crystallinity of Fe^0. Fig. 2b shows the XRD patterns of the ultrasonically irradiated nZVI@BC before and after RhB degradation, which show that the Fe^0 characteristic peak weakened after RhB degradation, and new peaks appeared at 47.3° and 60.4°, which were attributed to Fe_3O_4 and FeO, respectively, indicating that the chemical reaction happened during the RhB degradation, leading to the consumption of Fe^0 and the formation of iron oxides.[33] Furthermore, the structure of the used catalyst was almost identical to that of the fresh catalyst, suggesting that the ultrasonically irradiated nZVI@BC exhibited high stability.

The Raman spectra of the nZVI@BC prepared in the presence and absence of ultrasonic irradiation are shown in Fig. 2c. As can be seen, the D peak at 1350 cm^{-1} was attributed to sp^3-hybridized carbon with structural defects, and the G peak at 1590 cm^{-1} was attributed to sp^2-hybridized carbon in the graphite structure. The intensity ratio (I_D/I_G) reflects the defect and disorder degree of the carbon material.[34] The I_D/I_G values of the nZVI@BC prepared in the presence and absence of ultrasonic irradiation were 2.33 and 2.52, respectively, showing that the graphitization degree of the ultrasonically irradiated nZVI@BC was enhanced, which was good for improving the electronic transport performance.

In the initial stage of the heterogeneous Fenton-like reaction, the target pollutant is adsorbed on the catalyst surface; hence, the specific surface area and pore size of the catalyst influence the removal performance.[35] As shown in Fig. 2d, the adsorption isotherms of nZVI@BC prepared in the presence and absence of ultrasonic irradiation were class III isotherms, indicating that the interaction between N_2 molecules and the

Table 1 Specific surface analysis of the catalysts

Samples	S_{BET} ($m^2 g^{-1}$)	Pore volume ($cm^3 g^{-1}$)	Pore size (nm)
nZVI@BC (conventional method)	58.8	0.091	3.81
nZVI@BC (ultrasonic irradiation)	87.4	0.166	3.82

sample was poor. Meanwhile, the adsorption–desorption isotherms had obvious hysteresis loops, showing that the capillary coagulation phenomena had occurred, which corresponded to the mesoporous structure. The BET specific surface area of the nZVI@BC synthesized in the presence and absence of ultrasonic irradiation were measured to be 87.4 and 58.8 $m^2 g^{-1}$, respectively, suggesting the ultrasonically irradiated nZVI@BC had a larger specific surface area. Table 1 shows that the pore volume and pore size of the ultrasonically irradiated nZVI@BC were larger than those of nZVI@BC prepared in the absence of ultrasonic irradiation, revealing that nZVI@BC prepared under ultrasonic irradiation exhibited better adsorption performance.

Furthermore, the hysteresis loop of the ultrasonically irradiated nZVI@BC is shown in Fig. 3. The saturation magnetization value was 36.1 emu g^{-1}, indicating that it could be easily separated from the solution with a magnet.

3.2 Comparison of RhB removal in various systems

The RhB removal efficiency of different systems was investigated, as shown in Fig. 4. The RhB removal efficiency was poor in the systems of only BC (13.7%), nZVI (7.8%), conventional method synthesized nZVI@BC (28.2%) and ultrasonically irradiated nZVI@BC (36.4%). It is worth noting that the ultrasonically irradiated nZVI@BC exhibited better adsorption performance than nZVI@BC synthesized by the conventional method. The BC/H_2O_2 system did not contain nZVI; hence, it could not form a Fenton system, and its removal capacity was limited. BC could adsorb RhB in the solution, and H_2O_2 could be decomposed under light to release active free radicals for RhB degradation. The RhB removal efficiency in the $FeCl_3$/H_2O_2 system remained at a low level (41.2%), which is far lower than that of the nZVI@BC(ultrasonic irradiation)/H_2O_2 system (97.7%), demonstrating that the $FeCl_3$ salt itself had poor catalytic activity for RhB degradation, and the high efficiency of the nZVI@BC catalyst was not derived from the $FeCl_3$ salt. The RhB removal efficiencies of the three Fenton-like systems nZVI/H_2O_2, nZVI@BC(conventional method)/H_2O_2 and nZVI@BC(ultrasonic irradiation)/H_2O_2 were 78.6%, 93.4% and 97.7%, respectively. The Fe^0 particles were corroded in the solution, and the generated iron ions catalyzed H_2O_2 to produce lots of reactive radicals, including $^{\bullet}OH$ and $^{\bullet}O_2^-$, which rapidly and efficiently degraded RhB.

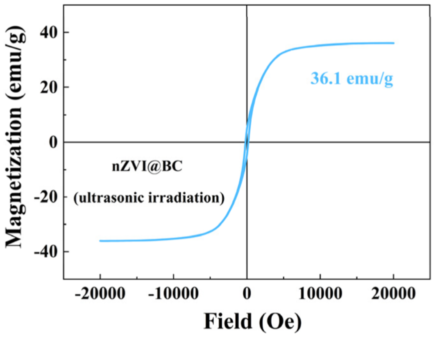

Fig. 3 Hysteresis loop of the nZVI@BC prepared in the presence of ultrasonic irradiation.

The nZVI@BC(ultrasonic irradiation)/H_2O_2 Fenton-like system exhibited the highest removal efficiency, which was because the nZVI@BC catalyst prepared under ultrasonic irradiation had a higher specific surface area and a higher porosity, which was conducive to adsorbing RhB in the solution. Furthermore, the cavitation effect and the mechanical shear force of ultrasound suppressed the agglomeration of nZVI particles. Hence, the nZVI@BC catalyst had a lower electron transfer resistance, more surface active sites were exposed for H_2O_2 activation, and more active radical substances were produced for RhB degradation. Hence, the nZVI@BC (ultrasonic irradiation)/H_2O_2 Fenton-like system was used for the subsequent degradation experiments.

3.3 Effect of the initial pH, catalyst dosage, H_2O_2 concentration and temperature on RhB degradation

Fig. 5a shows the effect of different pH values on RhB degradation. It can be seen that the removal efficiency gradually decreased with increasing pH value. When the pH value was 3, 5, 7, 9 and 11, the removal efficiency was 97.7%, 88.5%, 80.9%,

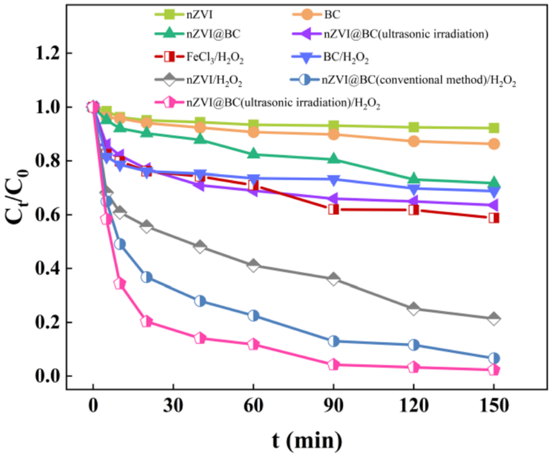

Fig. 4 Comparison of RhB removal in different systems. Reaction conditions: [catalyst] = 1.5 g L^{-1}, [H_2O_2] = 15 mM, [RhB] = 100 mg L^{-1}, T = 298 K and initial pH = 3.

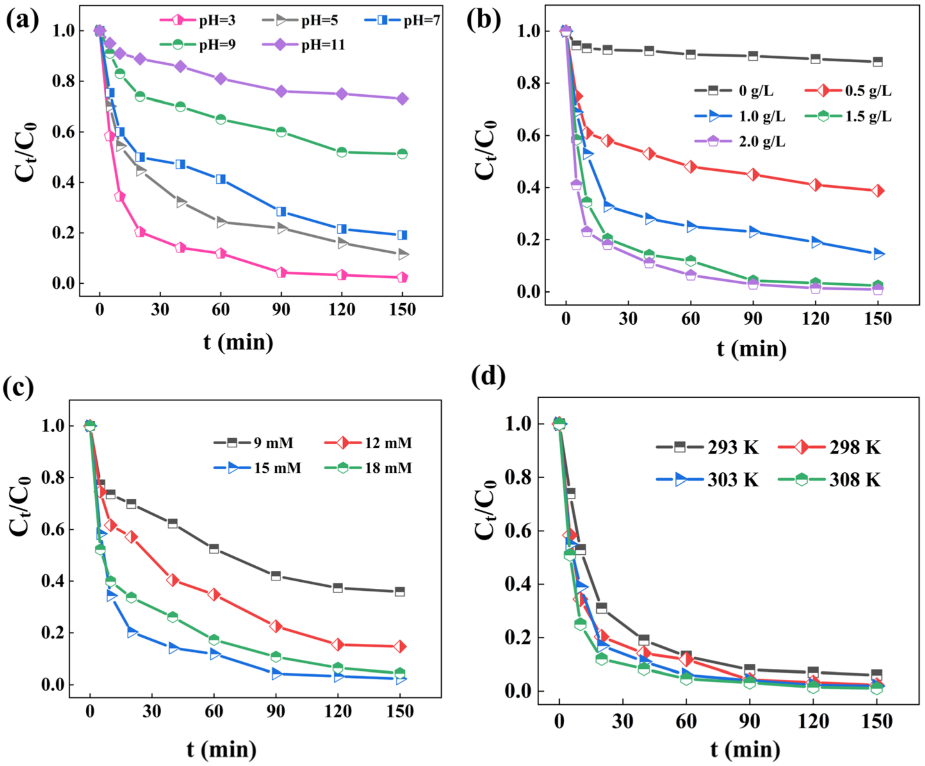

Fig. 5 Effect of the parameters on RhB degradation by the nZVI@BC(ultrasonic irradiation)/H_2O_2 Fenton-like system: (a) initial pH, (b) catalyst dosage, (c) H_2O_2 concentration, and (d) temperature. Except for the investigated parameter, the other parameters were fixed: [catalyst] = 1.5 g L^{-1}, [H_2O_2] = 15 mM, [RhB] = 100 mg L^{-1}, $T = 298$ K and initial pH = 3.

48.7% and 26.9%, respectively. Additionally, as the pH value varied from 3 to 7, the RhB removal efficiency still remained more than 80%. Furthermore, the traditional Fe^{2+}/H_2O_2 homogeneous Fenton system could only degrade pollutants under acidic conditions of pH 3. The nZVI@BC(ultrasonic irradiation)/H_2O_2 heterogeneous Fenton-like system had effectively broadened the applicable range of pH values. The acidic conditions prevented the formation of the oxide film on nZVI and contributed to the leaching of iron. Thus, Fe^{2+} ions were released into the system to catalyze H_2O_2 decomposition, which produced lots of $^{\bullet}OH$ free radicals for RhB degradation. When the pH value of the solution increased, the Fe^0 gradually transformed into the iron complex, forming the $Fe(OH)_3$ precipitate, which covered the active sites and decreased the catalytic activity for H_2O_2.

Fig. 5b shows the effect of the catalyst dosage on RhB degradation. When the dosage was 0, 0.5, 1.0, 1.5 and 2 g L^{-1}, the RhB degradation efficiency was 11.8%, 61.2%, 85.5%, 97.7% and 99.2%, respectively. With increasing catalyst dosage, the RhB degradation efficiency improved gradually. When the dosage was 0 g L^{-1}, the removal efficiency was less than 15%, indicating that H_2O_2 alone did not have a high removal capacity. The catalyst enhanced the decomposition of H_2O_2 to produce lots of $^{\bullet}OH$ for RhB degradation, and more catalyst also adsorbed more RhB on the surface, which was conducive to degrading RhB at the interface. However, when the catalyst dosage increased from 1.5 to 2.0 g L^{-1}, the increase in the degradation efficiency was very small, possibly because the excess Fe^{2+} ions consumed the $^{\bullet}OH$ free radicals ($Fe^{2+} + {}^{\bullet}OH \rightarrow Fe^{3+} + OH^-$), resulting in a decrease in the $^{\bullet}OH$ concentration. In addition, excessive catalyst would cause agglomeration, reducing the number of available active sites. Thus, 1.5 g L^{-1} was the optimal dosage for the catalyst.

Fig. 5c shows the effect of the H_2O_2 concentration on RhB degradation. It can be seen that when the H_2O_2 concentration was 9, 12, 15 and 18 mmol L^{-1}, the RhB degradation efficiency was 64.1%, 85.3%, 97.7% and 95.6%, respectively, suggesting that with increasing H_2O_2 concentration, the degradation efficiency first increased and then decreased, and adding excess H_2O_2 might lead to the quenching of free radicals. The highest removal efficiency was obtained when the H_2O_2 concentration was 15 mmol L^{-1}, which was used for subsequent experiments.

As can be seen in Fig. 5d, the nZVI@BC(ultrasonic irradiation)/H_2O_2 Fenton-like system exhibited a good RhB removal efficiency as the temperature varied from 293 K to 308 K, and the RhB degradation efficiency at all temperatures was over 90%. Furthermore, the RhB removal efficiency was enhanced and the degradation process was also accelerated with rising temperature, which was probably because a higher temperature provided more energy for the Fenton reaction and intensified the thermal motion of reaction molecules, increasing the collision probability to rapidly catalyze H_2O_2 decomposition;[36] hence, lots of $^{\bullet}OH$ free radicals were generated for RhB degradation.

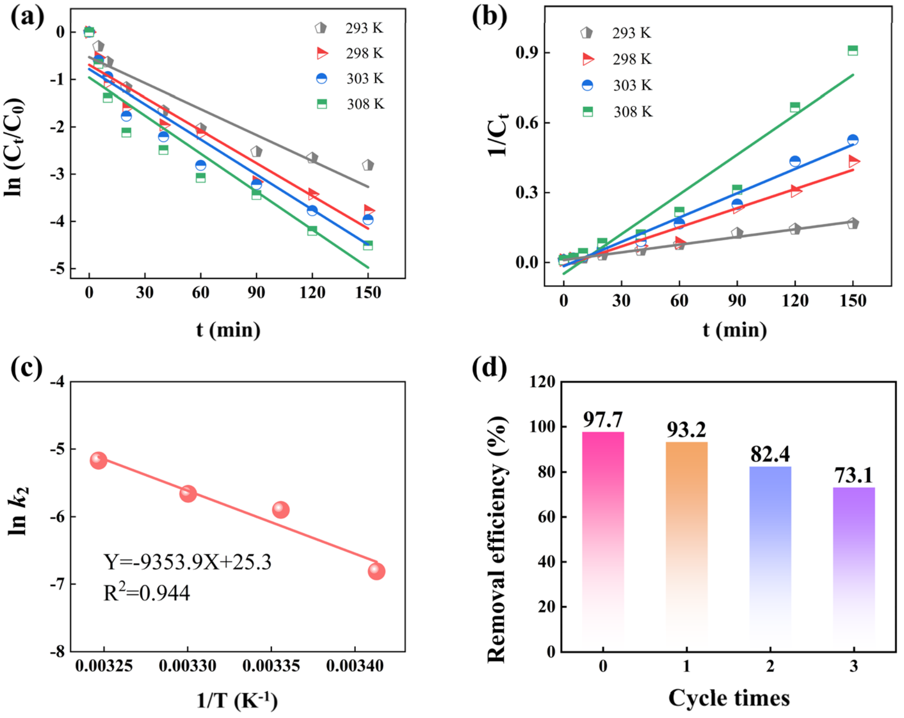

Fig. 6 (a) Linear fitting of classical first-order kinetics; (b) linear fitting of classical second-order kinetics; (c) linear fitting of the Arrhenius equation; and (d) reusability of the catalyst for the degradation of RhB. Experimental conditions: [catalyst] = 1.5 g L^{-1}, [H_2O_2] = 15 mM, [RhB] = 100 mg L^{-1}, $T = 298$ K and initial pH = 3.

3.4 Kinetics of RhB removal

To investigate the mechanisms of the nZVI@BC(ultrasonic irradiation)/H_2O_2 Fenton-like system for RhB degradation, the degradation data obtained at different temperatures were fitted by the classical first-order and second-order kinetic models, and the activation energy (E_a, J mol^{-1}) for the degradation reaction was calculated using the Arrhenius formula by plotting ln k *versus* $1/T$.

The classical kinetic model fitting plots are shown in Fig. 6a and b, and the corresponding parameters are listed in Table 2. Clearly, the R^2 values of the first-order kinetic model ranged from 0.884 to 0.913, while those of the second-order kinetic model ranged from 0.938 to 0.988. The second-order kinetic model showed a better fitting result. Therefore, the interaction between the catalyst and RhB involved both physical adsorption and chemical adsorption, and the reaction mechanism was primarily controlled by chemical adsorption.[37,38]

Table 2 Kinetic parameters for RhB degradation from the classical kinetic models

Temperature (K)	Classical first-order kinetic model		Classical second-order kinetic model	
	k_1 (min^{-1})	R^2	k_2 (L mg^{-1} min^{-1})	R^2
293	1.83×10^{-2}	0.874	1.10×10^{-3}	0.988
298	2.31×10^{-2}	0.913	2.74×10^{-3}	0.959
303	2.47×10^{-2}	0.890	3.48×10^{-3}	0.978
308	2.68×10^{-2}	0.884	5.69×10^{-3}	0.938

Additionally, based on the kinetic fitting results, the second-order kinetic rate constant, k_2, was used instead of k in the Arrhenius formula, and the plot of ln k_2 *versus* $1/T$ was constructed, which is shown in Fig. 6c. The value of E_a for RhB degradation was calculated to be 77.8 kJ mol^{-1}. Generally, chemical reactions require lots of energy to break chemical bonds, resulting in a high activation energy.[39]

3.5 Reusability of the catalyst for RhB degradation

To evaluate the reusability of the catalyst, the nZVI@BC was collected with a magnet after each degradation, and the used catalyst was washed with oxygen-free deionized water and ethanol and then regenerated by a 0.5 mol L^{-1} $NaBH_4$ solution. RhB was degraded using the recycled catalyst under the same reaction conditions. As seen in Fig. 6d, when the catalyst was recycled once, the RhB degradation efficiency decreased by only 4.5%. However, although the degradation efficiency decreased significantly in the subsequent cycles, it still remained above 70% after three cycling experiments, and the reason might be the consumption or deactivation of the active sites on the catalyst.[40]

3.6 Potential mechanisms for RhB degradation

3.6.1 Electrochemical experiments. The Tafel curve and Nyquist curve are shown in Fig. 7a and b, respectively. The corrosion potentials of the nZVI@BC prepared in the presence and absence of ultrasonic irradiation were −0.92 and −0.86 V, respectively, indicating that ultrasonically irradiated nZVI@BC had a higher electron transfer rate.[41] Similarly, the Nyquist

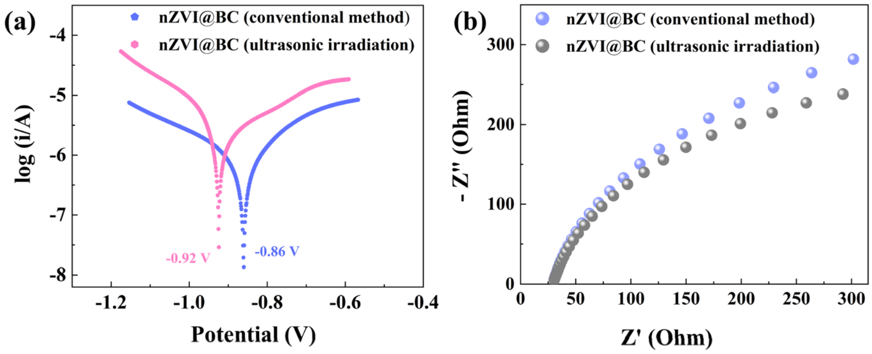

Fig. 7 (a) Steady-state Tafel curves and (b) Nyquist curves (experimental conditions: 0.5 mol L^{-1} Na_2SO_4 and $T = 298$ K).

curve showed that ultrasonically irradiated nZVI@BC had a smaller EIS radius, suggesting the ultrasonically irradiated nZVI@BC had a lower electron transfer resistance.[42] The cavitation effect and mechanical shear force of ultrasound inhibited the agglomeration of nZVI, broke the oxide film on the nZVI surface and exposed more surface active sites, which accelerated the electrochemical reaction, and the mechanical effect of ultrasound enhanced the physical adsorption and chemical bonding between nZVI and BC, forming a closer interfacial contact. According to the XRD and Raman characterization results, the nZVI@BC prepared under ultrasonic irradiation improved the crystallinity of Fe^0 and enhanced the graphitization degree of BC, which were favourable for strengthening the electron transport efficiency. In conclusion, ultrasound enhanced the electrochemical activity by modulating the nanostructure of nZVI@BC, which accelerated the consumption of nZVI, and the corrosion product, Fe^{2+} ions, facilitated the Fenton reaction.

3.6.2 XPS analysis. As shown in Fig. 8a, the nZVI@BC composite mainly contained the C, O and Fe elements, as analyzed using the XPS characterization technique. Combined with the XRD results, it could be inferred that the nZVI was successfully loaded onto BC. Importantly, a weak N 1s signal was detected at around 400 eV after the reaction, which was from the incompletely degraded RhB, indicating that the RhB molecules were adsorbed on the catalyst surface.

In the Fe 2p spectra (Fig. 8b), the characteristic peaks at 708.6, 711.3 and 713.4 eV corresponded to Fe^0, Fe^{2+} and Fe^{3+}, respectively,[43] indicating that the nZVI@BC contained Fe^0 and iron oxides. After the reaction, the characteristic peak of Fe^0 disappeared, suggesting that Fe^0 was oxidized to Fe^{2+} during the degradation. The generated Fe^{2+} ions catalyzed H_2O_2 molecules to produce a large number of free radicals for RhB degradation. Simultaneously, the Fe^{2+} ions were oxidized to Fe^{3+} ions, which were reduced to Fe^{2+} again by Fe^0, achieving the Fe^{2+} active species regeneration to maintain the efficiency of the Fenton

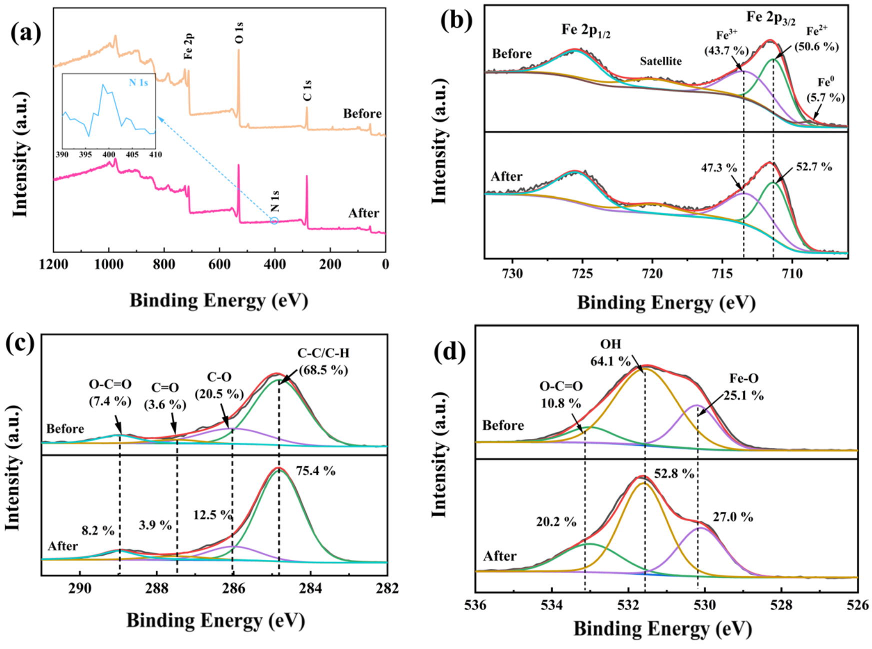

Fig. 8 XPS spectra of the ultrasonically irradiated nZVI@BC: (a) total survey scan spectra and high-resolution spectra of (b) Fe 2p, (c) C 1s, and (d) O 1s.

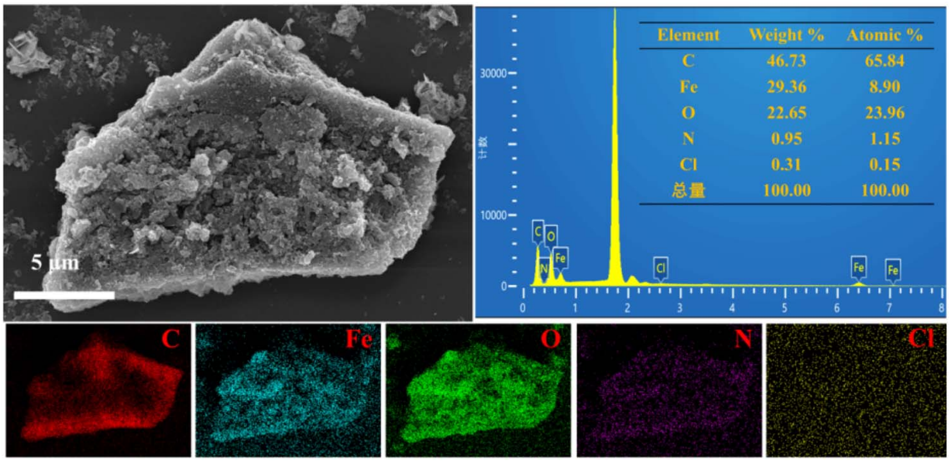

Element	Weight %	Atomic %
C	46.73	65.84
Fe	29.36	8.90
O	22.65	23.96
N	0.95	1.15
Cl	0.31	0.15
总量	100.00	100.00

Fig. 9 SEM image of the ultrasonically irradiated nZVI@BC and EDS elemental mapping after RhB degradation.

reaction. Hence, the number of Fe^{2+} and Fe^{3+} ions increased after the reaction, and the corresponding characteristic peak areas also increased.

In the C 1s spectra (Fig. 8c), the four characteristic peaks at 284.8, 286.1, 287.5 and 288.9 eV were attributed to C–C/C–H, C–O, C=O and O–C=O bonds, respectively. After the reaction, the O–C=O peak area increased because RhB molecules and the intermediate degradation products contained O–C=O groups, which were adsorbed on the catalyst surface.

As can be seen from the O 1s spectra (Fig. 8d), the characteristic peak at 530.2 eV represented the Fe–O bond, and the peak area increased after the reaction because nZVI was oxidized to iron oxides during the degradation process. The peaks at 531.5 and 533.1 eV represented the oxygen-containing groups –OH and O–C=O, respectively. Because the –OH groups were further oxidized to generate O–C=O groups during the reaction, the –OH peak area decreased and the O–C=O peak area increased after the reaction. Additionally, the BC material contained a certain amount of oxygen-containing functional groups (–OH and C=O) on its surface. These groups imparted a degree of hydrophilicity to the BC surface,[44] facilitating initial contact and wetting by the H_2O_2 solution. The polar oxidant (H_2O_2 in water) interacted with the pollutant at the BC-water interface and enhanced the subsequent oxidation.

3.6.3 SEM analysis after degradation. The SEM of the catalyst after degradation is shown in Fig. 9. The catalyst surface became rough after the reaction, and the nZVI particles were obviously aggregated together. EDS results showed that the catalyst contained Fe, O, C, N and Cl elements after degradation, and the N and Cl elements were from RhB molecules, indicating that RhB was adsorbed on the catalyst, which was consistent with the XPS analysis results. Furthermore, the content of the Fe element in the catalyst before and after degradation was 31.3% and 29.36%, respectively, which was basically unchanged, revealing that few Fe species in the solid catalyst were lost in the solution, and the catalyst had good stability.

3.6.4 Active species analysis for RhB degradation. The free radical signal capture experiments and EPR tests were conducted with benzoquinone (BQ) as the $^{\bullet}O_2^-$ capture agent and tertiary butanol (TBA) as the $^{\bullet}OH$ capture agent, and 5.5-dimethyl-1-pyrroline *N*-oxide (DMPO) was used as the capture agent for $^{\bullet}O_2^-$ and $^{\bullet}OH$. Fig. 10a shows that the RhB degradation efficiency decreased rapidly after adding the TBA agent,

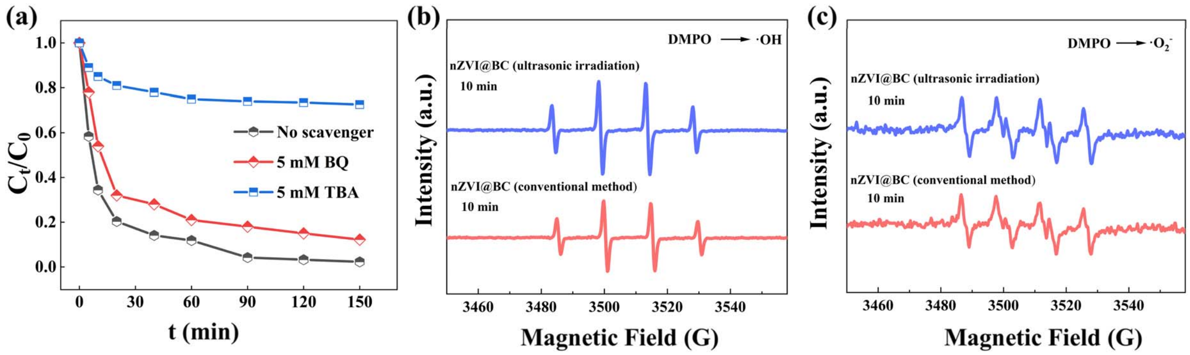

Fig. 10 (a) Effects of different free radical scavengers on the degradation of RhB in the nZVI@BC(ultrasonic irradiation)/H_2O_2 Fenton-like system. (b) and (c) EPR spectra of the free radicals. Experimental conditions: [catalyst] = 1.5 g L^{-1}, [H_2O_2] = 15 mM, [RhB] = 100 mg L^{-1}, T = 298 K and initial pH = 3.

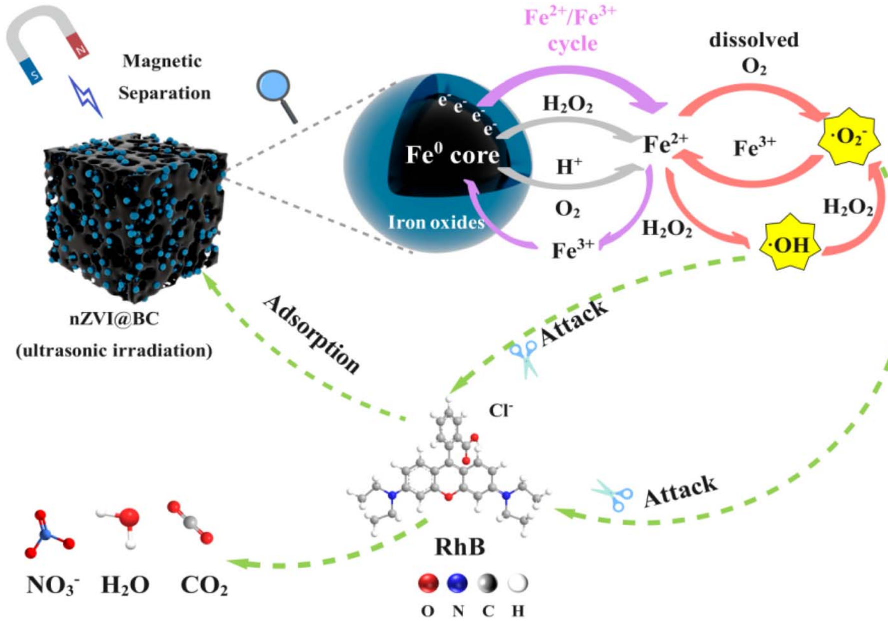

Fig. 11 Mechanisms of RhB degradation in the Fenton-like system.

which was only 27.4%. In addition, the addition of BQ to capture $^{\bullet}O_2^-$ had a little inhibitory effect on RhB degradation, and the RhB removal efficiency still reached 87.8%, suggesting that the ·OH free radicals played a major role in RhB removal. As shown in Fig. 10b and c, the free radical signals in the nZVI@BC(conventional method)/H_2O_2 and nZVI@BC(ultrasonic irradiation)/H_2O_2 Fenton-like systems were detected after 10 min of the reaction. The $^{\bullet}OH$ signal peak was stronger in the nZVI@BC(ultrasonic irradiation)/H_2O_2 system, demonstrating that the ultrasonically irradiated nZVI@BC activated H_2O_2 to produce more $^{\bullet}OH$ free radicals. The signal intensity of $^{\bullet}O_2^-$ free radicals in the two systems did not have an obvious difference, probably because $^{\bullet}O_2^-$ free radicals were not the main active substance, and the number of $^{\bullet}O_2^-$ free radicals was very low in the two systems. These results indicated that ultrasonically irradiated nZVI@BC exhibited better catalytic performance, and $^{\bullet}OH$ free radicals were the main active species in RhB removal.[45]

In summary, the RhB degradation mechanism of the nZVI@BC(ultrasonic irradiation)/H_2O_2 Fenton-like system was inferred as follows: firstly, RhB molecules were adsorbed onto the surface of the catalyst. BC adsorbed RhB molecules through physical adsorption due to its large specific surface area. The –COOH and –OH groups in BC also formed hydrogen bonds with the N atoms in RhB molecules. Then, the nZVI particles were corroded in solution to generate Fe^{2+} (eqn (4) and (5)), and the Fe^{2+} catalyzed the decomposition of H_2O_2 to produce $^{\bullet}OH$ active free radicals for RhB removal, while the Fe^{2+} ions were oxidized to Fe^{3+} (eqn (6)). Additionally, the generated Fe^{3+} was reduced back to Fe^{2+} by nZVI (eqn (7)), which sustained the Fenton reaction and continuously produced $^{\bullet}OH$ free radicals for RhB degradation. Furthermore, the Fe^{2+} ions reacted with the few dissolved O_2 in the solution to produce superoxide radicals, $^{\bullet}O_2^-$ (eqn (8)). Finally, lots of active free radicals entered the system to effectively degrade RhB molecules. The degradation mechanism is shown in Fig. 11.

$$2Fe^0 + O_2 + 4H^+ \rightarrow 2Fe^{2+} + 2H_2O \tag{4}$$

$$Fe^0 + H_2O_2 + 2H^+ \rightarrow Fe^{2+} + 2H_2O \tag{5}$$

$$Fe^{2+} + H_2O_2 \rightarrow Fe^{3+} + {}^{\bullet}OH + OH^- \tag{6}$$

$$Fe^{3+} + Fe^0 \rightarrow 2Fe^{2+} \tag{7}$$

$$Fe^{2+} + O_2 \rightarrow Fe^{3+} + {}^{\bullet}O_2^- \tag{8}$$

4. Conclusion

In this study, the nZVI@BC catalyst was prepared using the ultrasound-assisted liquid-phase reduction method. The characterization results showed that the ultrasonically irradiated nZVI@BC could prevent the agglomeration of nZVI, increase the crystallinity of Fe^0 and enhance the graphitization degree of BC. Electrochemical experiments revealed that the nZVI@BC prepared under ultrasonic irradiation had a higher electron transfer rate, showing that the ultrasonically irradiated nZVI@BC was advantageous for the catalytic degradation of RhB. The RhB removal efficiency was 97.7% under the conditions of an initial pH of 3, an H_2O_2 concentration of 15 mmol L^{-1}, a catalyst dosage of 1.5 g L^{-1} and a temperature of 298 K. Meanwhile, the second-order kinetic model showed a better fitting result. Therefore, chemical adsorption primarily controlled the degradation reaction. The activation energy was calculated to be 77.8 kJ mol^{-1}. According to the quenching experiments and EPR spectra, two kinds of free radicals ($^{\bullet}O_2^-$

and $^{\bullet}OH$) were observed, and $^{\bullet}OH$ was the main free radical for RhB removal. After three reuse cycles of nZVI@BC, its removal efficiency for RhB was still more than 70%, showing good recycling performance. This work provides scientific insights into enhancing the catalytic performance in Fenton-like reactions.

Conflicts of interest

The authors declare no conflicts of interest.

Data availability

All data generated or analyzed during this study are included in this published article.

Acknowledgements

The authors acknowledge the Nanjiang Technology Project (2023AB028), the Patent transformation and application and industrialization project (BTSCJGJ-ZSCQ-2024004), the President's Fund Major Project Cultivation Special (TDZKZD202502), the State Key Laboratory of Chemical Resource Engineering (CRUZD2301), the presidential research fund of Tarim University (TDZKSS202127), the Talent Development Plan for Top Scientific and Technological Leading Talents Project (XJRC-2025-BTKJ-PY-KJLJ-007) and the National Natural Science Foundation Regional Fund of China (21868035) for the financial support to this study.

References

1 T. Das, M. Kaur, N. Kaur, P. K. Bhowmik, H. Han, H. S. Sohal and F. M. Husain, Greener and magnetic Fe_3O_4 nanoparticles as a recyclable catalyst for Knoevenagel condensation and degradation of industrial Congo red dye, *Green Process. Synth.*, 2025, **14**, 20240257.
2 F. Bibi, M. Jamshaid, W. A. Al-onazi, A. Kalsoom, M. A. Hossain, R. Iqbal, M. S. Elshikh and S. Iqbal, Design of Sm-doped $GdFeO_3$/g-C_3N_4 heterostructure Z-scheme photo-catalyst for the elimination of malachite green dye from industrial water, *Opt. Mater.*, 2025, **160**, 116696.
3 J. Guo, L. Fu, R. Gao, Y. Zhang, C. Yin and B. Xue, Efficiency removal of rhodamine B by MoS_2/magnetic potato residues biochar: Performance and mechanism, *Ind. Crop Prod.*, 2025, **233**, 121390.
4 L. Qiu, H. Li, W. Xu, R. Zhu and F. Ouyang, TiO_2 Catalysts Co-Modified with Bi, F, SnO_2, and SiO_2 for Photocatalytic Degradation of Rhodamine B Under Simulated Sunlight, *Catalysts*, 2024, **14**, 735.
5 K. H. H. Aziz, F. S. Mustafa, M. A. H. Karim and S. Hama, Biochar-based catalysts: an efficient and sustainable approach for water remediation from organic pollutants *via* advanced oxidation processes, *J. Environ. Manage.*, 2025, **390**, 126245.
6 K. Yin, Y. Tang, Z. Li, H. Zhao, X. Xu, Q. Li, Q. Yue, Y. Gao and B. Gao, Powerful Fenton-like reactions derived from montmorillonite modulated Co single atom: Key role of heterogeneous high-valent Co (IV)-oxo, *Water Res.*, 2025, **285**, 124130.
7 X. Li, M. Liu, L. Wen, R. Li, Y. Liu, S. Yang, D. Ding, Y. Chen, R. Chen and S. Xu, Synergism between Activated Carbon and Fenton Reaction for Organic Pollutant Degradation: The Hitherto Overlooked Role of Dynamic Single-Atom Sites, *Environ. Sci. Technol.*, 2025, **59**, 13458–13469.
8 S. R. Irudhaya and J. Adhish, Nanoscale transformation in CuS Fenton-like catalyst for highly selective and enhanced dye degradation, *J. Photochem. Photobiol., A*, 2021, **410**, 113158.
9 L. Dai, B. Li, H. Xu, W. Wang, S. Zhang, Y. Xu, S. Qi, X. He and L. Jin, Magnetic nanoreactor Fe_3O_4@HNTs as heterogeneous Fenton-like catalyst for acid fuchsin degradation: Efficiency, kinetics and mechanism, *J. Phys. Chem. Solids*, 2023, **180**, 111445.
10 S. Wang, H. Yang, X. Kang and Y. Yang, Enhanced Fenton-like reactions *via* interface electron reconstruction in low-crystallinity FeCo bimetallic metal-organic frameworks: Bidirectional control of Fe (III) and Co (II) sites, *J. Colloid Interface Sci.*, 2025, **678**, 168–179.
11 S. Li, H. Wang, C. Qiu, J. Ren, Y. Peng, Y. Liu, F. Dong and Z. Bian, Electronic structure regulation of Fe single atom coordinated nitrogen doping MoS_2 catalyst enhances the Fenton-like reaction efficient for organic pollutant control, *J. Hazard. Mater.*, 2024, **467**, 133756.
12 K. Yin, L. Peng, D. Chen, S. Liu, Y. Zhang, B. Gao, K. Fu, Y. Shang and X. Xu, High-loading of well dispersed single-atom catalysts derived from Fe-rich marine algae for boosting Fenton-like reaction: Role identification of iron center and catalytic mechanisms, *Appl. Catal. B Environ.*, 2023, **336**, 122951.
13 Z. Bao, J. Li, X. Wang, S. Luo, N. Du, N. Gao and Y. Liu, Nano zero-valent iron with a self-forming Co-catalytic surface for enhanced Fenton-like reactions, *Environ. Res.*, 2025, **267**, 120736.
14 Y. Yang, L. Xu, W. Li, W. Fan, S. Song and J. Yang, Adsorption and degradation of sulfadiazine over nanoscale zero-valent iron encapsulated in three-dimensional graphene network through oxygen-driven heterogeneous Fenton-like reactions, *Appl. Catal. B Environ.*, 2019, **259**, 118057.
15 Z. Ning, B. Xu, W. Zhong, C. Liu, X. Qin, W. Feng and L. Zhu, Preparation of phosphoric acid modified antibiotic mycelial residues biochar: Loading of nano zero-valent iron and promotion on biogas production, *Bioresour. Technol.*, 2022, **348**, 126801.
16 A. Gil, M. J. Amiri, J. A. Koupai and S. Eslamian, Adsorption/reduction of Hg(II) and Pb(II) from aqueous solutions by using bone ash/nZVI composite: effects of aging time, Fe loading quantity and co-existing ions, *Environ. Sci. Pollut. Res.*, 2018, **25**, 2814–2829.
17 M. Cheng and P. Hu, Graphitic carbon nitride (g-C_3N_4) loaded nanoscale zero-valent iron (nZVI) composites for enhanced hexavalent chromium removal: The role of g-C_3N_4, performance and mechanistic study, *Inorg. Chem. Commun.*, 2025, **175**, 114161.

18 M. Che, J. Xiao, S. Zhang, C. Shan, Z. Zhao, R. Huang, Y. Zhou, M. Cui, W. Qi and R. Su, A Kirkendall strategy for the efficient degradation of trichloroethylene from groundwater using cellulose nanofiber-supported sulfidated nZVI, *Chem. Eng. J.*, 2024, **501**, 157816.

19 Y. Yang, Y. Xu, D. Zhong, Q. Qiao and H. Zeng, Efficient removal of Cr(VI) by chitosan cross-linked bentonite loaded nano-zero-valent iron composite: Performance and mechanism, *J. Hazard. Mater.*, 2024, **480**, 136183.

20 J. Hu and P. Hu, Evaluation of a novel kaolinite loaded sulfidized nZVI aggregates for removing Cr(VI) and Cd(II) in water: New sulfurization strategy, morphological control, performance, and synergistic mechanisms, *Sep. Purif. Technol.*, 2025, **363**, 132171.

21 D. Tesnim, A. M. Díez, B. A. Hédi, M. Á. Sanroman and M. Pazos, Sustainable removal of antipyrine from wastewater *via* an Eco-Friendly heterogeneous Electro-Fenton-like process employing Zero-Valent iron nanoparticles loaded activated carbon, *Chem. Eng. J.*, 2024, **493**, 152494.

22 G. Wang, X. Zhao, W. Luo, J. Yuan, Y. Guo, X. Ji, W. Hu, M. Li and Z. Teng, Noval porous phosphate-solubilizing bacteria beads loaded with BC/nZVI enhanced the transformation of lead fractions and its microecological regulation mechanism in soil, *J. Hazard. Mater.*, 2022, **437**, 129402.

23 A. Talati, M. Haghighi and I. Ghasemi, Enhanced synthesis of plasmonic mesoporous Ag-doped $ZnAl_2O_4$ nanophotocatalyst *via* synergistic ultrasound and microwave irradiation for efficient organic dye degradation, *Adv. Powder Technol.*, 2025, **36**, 104855.

24 D. Zhao, Y. Liu and C. Wu, Adsorption of Cr(VI) polluted water by Fe_3O_4@SiO_2-APTMS nanocomposites prepared in the presence of ultrasonic irradiation for sustainable water resources utilization, *Ultrason. Sonochem.*, 2023, **96**, 106439.

25 M. Pirsaheb, S. Moradi, M. Shahlaei, X. Wang and N. Farhadian, Ultrasonic Enhanced Zero-Valent Iron-Based Fenton Reaction for Ciprofloxacin Removal under Aerobic Condition, *Environ. Processes*, 2020, **7**, 227–241.

26 R. Kareem, A. Afkhami and K. H. H. Aziz, Synthesis of a novel magnetic biochar composite enhanced with polyaniline for high-performance adsorption of heavy metals: focus on Hg(II) and Cu(II), *RSC Adv.*, 2025, **15**, 20309–20320.

27 R. Fu, Y. Liu, Z. Lou, Z. Wang, S. Baig and X. Xu, Adsorptive removal of Pb(II) by magnetic activated carbon incorporated with amino groups from aqueous solutions, *J. Taiwan Inst. Chem. Eng.*, 2016, **62**, 247–258.

28 L. Liu, R. Yu, S. Zhao, X. Cao, X. Zhang and S. Bai, Heterogeneous Fenton system driven by iron-loaded sludge biochar for sulfamethoxazole-containing wastewater treatment, *J. Environ. Manage.*, 2023, **335**, 117576.

29 C. Liu, J. Lu, Y. Tan, B. Chen and P. Yang, Removal of U(VI) from wastewater by sulfhydryl-functionalized biomass carbon supported nano-zero-valent iron through synergistic effect of adsorption and reduction, *Mater. Sci. Eng., B*, 2022, **284**, 115891.

30 O. Falyouna, K. Bensaida, I. Maamoun, U. P. M. Ashik, A. Tahara, K. Tanaka, N. Aoyagi, Y. Sugihara and O. Eljamal, Synthesis of hybrid magnesium hydroxide/magnesium oxide nanorods $[Mg(OH)_2/MgO]$ for prompt and efficient adsorption of ciprofloxacin from aqueous solutions, *J. Clean. Prod.*, 2022, **342**, 130949.

31 D. Zhao, Y. Liu and C. Wu, Reductive dechlorination of 2,4-dichlorophenol by using MWCNTs-Pd/Fe nanocomposites prepared in the presence of ultrasonic irradiation, *Ultrason. Sonochem.*, 2024, **105**, 106871.

32 H. Qiao, J. Hu, H. Xu and Y. Zhao, Study of the nano zero-valent iron stabilized by carboxymethyl cellulose loaded on biochar for remediation of Cr(VI)-contaminated groundwater, *Sep. Purif. Technol.*, 2025, **353**, 128494.

33 C. Li, Y. Hu, C. Yan, Y. Zhang, Y. Fan, D. Ji, B. Wang and L. Zhu, Biochar supported modified nZVI for effective remediation of hexavalent chromium: Enhanced performance and remediation mechanism, *J. Environ. Chem. Eng.*, 2024, **12**, 114410.

34 C. Wang, R. Sun and R. Huang, Highly dispersed iron-doped biochar derived from sawdust for Fenton-like degradation of toxic dyes, *J. Clean. Prod.*, 2021, **297**, 126681.

35 C. Li, X. Tan and J. Ma, Concerted high innergenerated-H_2O_2 photocatalysis and photo-Fenton degradation of organic pollutants over SCNO@CdS, *J. Photochem. Photobiol., A*, 2021, **420**, 113477.

36 X. Zou, T. Zhang, Y. Dong, C. Hu, L. Yin, Y. Zheng, M. Li, X. Xiao and W. Hui, Enhanced removal of sulfonamide antibiotics in water using high-performance S-nZVI/BC derived from rice straw, *J. Environ. Manage.*, 2025, **373**, 123955.

37 L. Qian, X. Shang, B. Zhang, W. Zhang, A. Su, Y. Chen, D. Ouyang, L. Han, J. Yan and M. Chen, Enhanced removal of Cr(VI) by silicon rich biochar-supported nanoscale zero-valent iron, *Chemosphere*, 2019, **215**, 739–745.

38 L. Tan, J. Xu, X. Xue, Z. Lou, J. Zhu, S. A. Baig and X. Xu, Multifunctional nanocomposite Fe_3O_4@SiO_2-mPD/SP for selective removal of Pb(II) and Cr(VI) from aqueous solutions, *RSC Adv.*, 2014, **4**, 45920–45929.

39 F. Sang, Z. Yin, W. Wang, E. Almatrafi, Y. Wang, B. Zhao, J. Gong, C. Zhou, C. Zhang, G. Zeng and B. Song, Degradation of ciprofloxacin using heterogeneous Fenton catalysts derived from natural pyrite and rice straw biochar, *J. Clean. Prod.*, 2022, **378**, 134459.

40 G. Barzegar, S. Jorfi, V. Zarezade, M. Khatebasreh, F. Mehdipour and F. Ghanbari, 4-Chlorophenol degradation using ultrasound/peroxymonosulfate/nanoscale zero valent iron: Reusability, identification of degradation intermediates and potential application for real wastewater, *Chemosphere*, 2018, **201**, 370–379.

41 X. Yang, X. Dai, T. Jian and W. Tian, Enhanced adsorption and reduction of Pb(II) from aqueous solution by sulfide-modified nanoscale zerovalent iron: characterization, kinetics and mechanisms, *Inorg. Chem. Commun.*, 2024, **170**, 113496.

42 Y. Pei, W. Cheng, R. Liu, H. Di, Y. Jiang, C. Zheng and Z. Jiang, Synergistic effect and mechanism of nZVI/LDH composites adsorption coupled reduction of nitrate in micro-polluted water, *J. Hazard. Mater.*, 2023, **464**, 133023.

43 X. Yang, X. Li, X. Wang, Y. Mu and W. Tian, Magnetic triiron tetraoxide/biochar-loaded nanoscale zero-valent iron for chromium(VI) removal from aqueous solution, *J. Taiwan Inst. Chem. Eng.*, 2024, **159**, 105458.

44 J. Gao, D. Han, Y. Xu, Y. Liu and J. Shang, Persulfate activation by sulfide-modified nanoscale iron supported by biochar (S-nZVI/BC) for degradation of ciprofloxacin, *Sep. Purif. Technol.*, 2020, **235**, 116202.

45 X. Sun, X. Ni, X. Wang and D. Xu, Preparation of zero-valent iron-based composite catalyst with red mud and scrap tire as starting materials for Fenton-like degradation of methyl blue, *Surf. Interfaces*, 2022, **31**, 102053.